engineering proceedings

MDPI

Proceedings Paper

An In-Depth Analytical Study of Switching States of Direct Torque Control Algorithm for Induction Motor over the Entire Speed Range †

Mussaab M. Alshbib [1,*], Mohamed Elgbaily [2,3] and Fatih Anayi [2]

[1] Mechatronics & Laboratory Engineering Department, Sham University, Azez City, Aleppo, Syria
[2] Wolfson Centre for Magnetics, School of Engineering, Cardiff University, Cardiff CF24 3AA, UK; elgbailymm@cardiff.ac.uk (M.E.); anayi@cardiff.ac.uk (F.A.)
[3] Instrumentation & Electrical Division, Gas Transmission and Supply Department, Sirte Oil Company for Production, Manufacturing of Oil and Gas, Brega, Libya
* Correspondence: dr.mussaab.alshbib@shamuniversity.com; Tel.: +905394618937
† Presented at 1st International Electronic Conference on Machines and Applications, 15–30 September 2022; Available online: https://iecma2021.sciforum.net.

Abstract: In this paper, a full analysis of the Voltage Vectors (VVs) in DTC algorithm is presented. The analytical analysis showed that the application of specific VVs results in false switching states called Uncontrollable Angles (UCAs). A robust scheme that ensures the elimination of (UCAs) is proposed for medium and high speeds with (18) subsectors (SSs). Simulation results were obtained and validated by using MATLAB/Simulin.

Keywords: Adjustable speed drives; direct torque control (DTC); voltage source inverter; discrete space vector modulation (SVM); Lookup table (LUT).

Citation: Alshbib, M.M.; Elgbaily, M.; Anayi, F. An In-Depth Analytical Study of Switching States of Direct Torque Control Algorithm for Induction Motor over the Entire Speed Range. *Eng. Proc.* **2022**, *4*, x. https://doi.org/10.3390/xxxxx

Published: date

1. Introduction

Direct torque control (DTC) characterized by fast dynamic response, structural simplicity, and much simpler than the FOC [1–3]. Several improvements have been made to overcome problems associated with the DTC drive such as high torque ripple in particular [4]. Reference [5] provided an in-depth study of the VVs effect on the state variables issue over the entire speed range in terms of UnAs. To select the appropriate VV, a new approach is initially introduced by inserting the zero VV along with the selected one[6]. Research [7] eliminated the zero VVs during torque dynamics to establish a fast torque response in the transient state. A modified LUT for DTC of three-level dual VSI fed open-ended winding IM drive was proposed in [8], where the VVs selection for lower hysteresis boundary conditions were restructured with null voltages. Authors in [9] used the concept of virtual vectors for a seven-phase IM where the torque ripple in different operation conditions was investigated. A universal LUT is proposed for OW-PMSM drives under different conditions of the dc-link voltage ratio [10–12]. The proposed strategy effectively optimized the duty ratio of fundamental VV to minimize the error between reference VV and final VV imposed on motor terminals. A duty-ratio regulator that considers the operating speed impact on the torque deviation of the active voltage vectors was proposed in [12]. This article suggests an enhanced, simple, and effective DTFRC strategy that aims to eliminate the UnAs over the wide speed range. The proposed method, which uses (18) SSs for the rotor at medium and high speeds, overcomes the conventional (6) sectors DTRFC in terms of the UnAs. Simulations and experimental results are presented to show and compare the effectiveness of the proposed (18) SSs scheme in DTRFC algorithm of IM.

2. Theoretical Background

2.1. Analytical Modeling

The basic principle of DTRFC is summed up in the instantaneous control of both rotor flux and the torque using intermediate loops without current control ones. the two components of the rotor flux vector of the rotor are estimated in the stator reference frame (α^s-β^s) as the following:

$$\Phi^s_{r\alpha}=\frac{L_r}{L_m}(\Phi^s_{s\alpha}-\sigma L_s i^s_{s\alpha}) \quad (1)$$

$$\Phi^s_{r\alpha(\beta)}=\frac{L_r}{L_m}(\Phi^s_{s\alpha(\beta)}-\sigma L_s i^s_{s\alpha(\beta)}) \quad (2)$$

where L_m is the mutual inductance. L_s, and L_r are the stator and rotor self inductance respectively. σ is the leakage factor.

The rotor flux vector will be oriented according to α-coordinate axis. Thus, the imaginary component of the rotor flux vector will be zero, i.e.,: $\Phi_{r\beta}=0$, $\Phi_r=\Phi_{r\alpha}$. The derivatives of two controlled variables (Φ_r, Tem) are known as [5]:

$$S_{\Phi_r}=k_{\Phi_r}(\Phi_{r\_ref}-\Phi_r)-[\frac{L_m}{\sigma L_s\tau_r}\mathrm{Re}(\underline{\Phi}_s)-(\frac{1}{\sigma\tau_r})\Phi_r] \quad (3)$$

$$\frac{dS_{\Phi_r}}{dt}=-\frac{d\Phi_r}{dt}(k_{\Phi_r}-\frac{1}{\sigma\tau_r})-\frac{L_m}{\sigma L_s\tau_r}[\mathrm{Re}(\underline{V}_s-R_s\underline{i}_s-j\omega_s\underline{\Phi}_s)] \quad (4)$$

$$\frac{dS_{T_{em}}}{dt}=-\frac{dT_{em\_est}}{dt}=(\frac{1}{\sigma\tau_s}+\frac{1}{\sigma\tau_r})T_{em}-\frac{pL_m}{\sigma L_s L_r}\mathrm{Im}[\underline{V}_s\underline{\Phi}^*_r-j\omega\underline{\Phi}_s\underline{\Phi}^*_r] \quad (5)$$

where k_{Φ_r} is an optional positive constant. Depending on the previous equations, the block diagram of the DTRFC algorithm can be constructed.

To enhance the performance at medium and high speeds, a transition will be allowed between the conventional strategy with (6) sectors for the low-speed range, and the improved strategy with (18) SSs (for medium and high speeds) as shown in Figure 1.

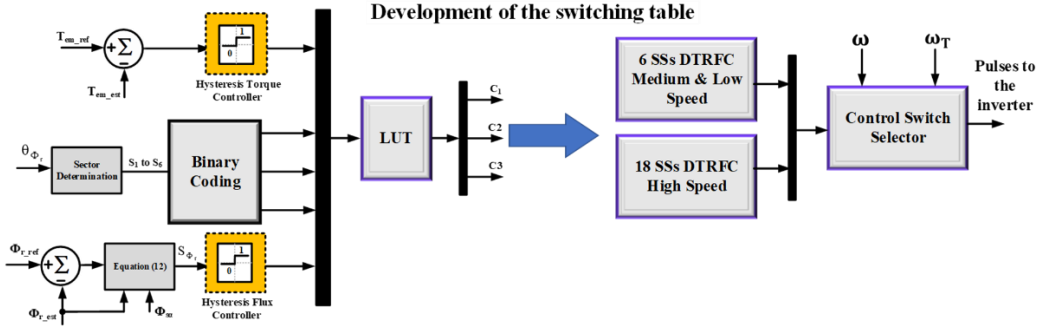

Figure 1. Block diagram of the conventional DTC and improved strategies over wide speed range.

2.2. Determination of the UnAs Values for Low and High Speeds

Depending on the equations (2) and (3), the effect of applying the two vectors V_{i+1}, V_{i-1} on $dS_{\Phi r}$ at low speed (20% ω_n) and V_{i+2}, V_{i-2} at high speed were analyzed. There are two UCAs at low speed and high speed with value of each $\pi/69$[rad/s] and $\pi/94$[rad/s], Respectively. In addition, the analysis is achieved for the two VVs (V_{i+1}, V_{i+2}) on dS_{Tem} at high speed. There are two UCAs. Each of them has a value equals $\pi/13$[rad/s] (22%) of the sector. Table 1 summarizes the values of the UnAs for each ($dS_{\Phi r}$, dS_{Tem}) over the entire speed range.

Table 1. Values of UnAs over the entire speed for DTRFC scheme.

Change of Error	Voltage Vector	Low Speed (20% ω_n(r/s)	High Speed (75% ω_n(r/s)	UnAs (Ratio of Sector)
dS_{Φ_r}	V_{i+1} or V_{i+2}	$\frac{\pi}{69}$ (rad)	$\frac{\pi}{94}$ (rad)	(3% to 4%) begin and end of sector
	V_{i-1} or V_{i-2}	$\frac{\pi}{69}$ (rad)	$\frac{\pi}{94}$ (rad)	(3% to 4%) begin and end of sector
$dS_{T_{em}}$	V_{i+2}	0(rad)	$\frac{\pi}{13}$ (rad)	(22%) begin of sector
	V_{i+1}	0(rad)	$\frac{\pi}{13}$ (rad)	(22%) end of sector

2.3. The Improved Strategy (18) SSs DTRFC Strategy for Medium-High Speeds

The proposed strategy is based on dividing the path of the rotor flux into (18) unequal SSs. Every three subsequent sectors will repeat the same distance after the previous three SSs. Depending on Equations (2) and (3), the position of the error change for the rotor flux and torque for a high speed (75% ω_n) were analyzed in order to devise the improved lookup table. The LUT for the improved strategy is shown in Table 2.

Table 1. The LUT of the improved strategy for (18) SSs

C_{Φ_r}	**0**	**1**	**0**	**1**	C_{Φ_r}	**0**	**1**	**0**	**1**
$C_{T_{em}}$	0	0	1	1	$C_{T_{em}}$	0	0	1	1
SS (1)	V_5	V_6	V_3	V_2	SS (16)	V_4	V_5	V_2	V_1
SS (2)	V_5	V_1	V_3	V_3	SS (17)	V_5	V_6	V_2	V_2
SS (3)	V_6	V_1	V_4	V_3	SS (18)	V_5	V_6	V_3	V_2

For the rest of the SSs, the applied vectors can be known by increasing the vector index by (1) when moving between SSs according to the following sequence:

- The first, fourth, seventh, tenth, thirteenth, and sixteenth SSs.
- The second, fifth, eighth, eleventh, fourteenth, and seventeenth SSs
- The third, sixth, ninth, twelfth, fifteenth, and eighteenth SSs.

2.4. Determination of the Transition Speed ωT between the Traditional and the Proposed Strategy

It is important to determine the speed at which UnAs start to appear, i.e., the transition speed ω_T. An increment was given to the angle $\theta_{\Phi r,}$ so it scans the entire sector. The speed was given a value starting from zero within an iterative loop during which the two components ($V_{s\alpha}$, $V_{s\beta}$) were calculated. The derivatives ($dS_{\Phi r}$, dS_{Tem}) were calculated according to the two equations (2&3). The speed range at which UnAs disappeared were within (0:55% ω_n), or (0:155[rad/s]). However, if the speed exceeds (155/rad/s), UnAs start to appear.

3. Simulation Results and Discussion

By simulating the proposed block diagram, in MATALB/Simulink environment, the simulation results are obtained in Figure 2. The speed of (180[rad/s]) which equals (63% ω_n) was chosen as a transition value between the conventional strategy and the improved one (18 SSs). The transition to the improved strategy was allowed with a chosen high speed (195[rad/s]) at (3[s]). A good regulation process around the reference values ($\Phi_{r\text{-}ref}$ = 0.945[Wb], $T_{em\text{-}ref}$ = 1.76[N.m]) could be achieved. The transition speed ω_T = 155[rad/s] was

the minimum value that ensured the absence of UnAs due to the correct selection of VVs according to the improved LUT in Table 2.

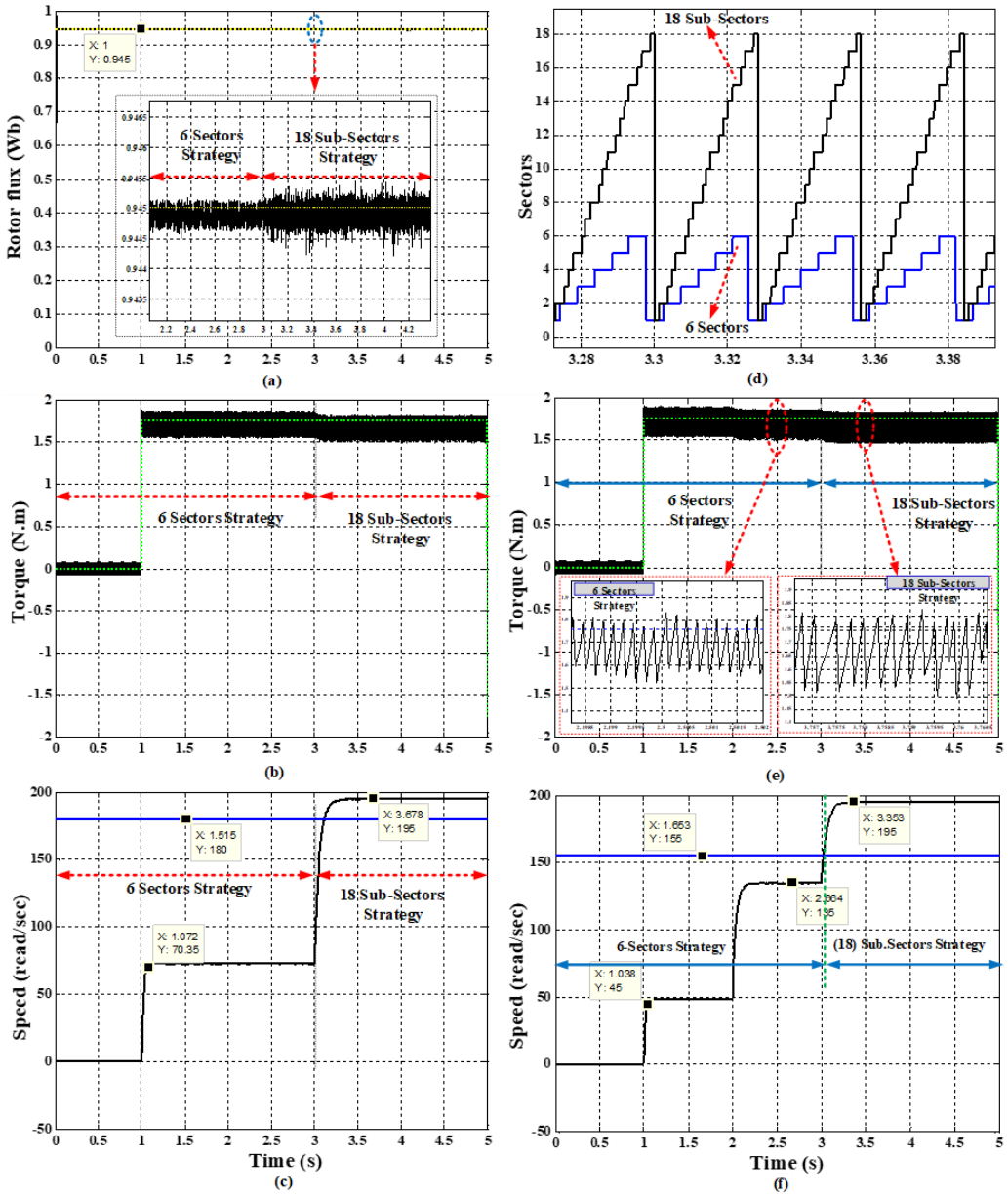

Figure 2. Simulation results of the improved and conventional strategy: (**a**): rotor flux, (**b**): torque response, (**c**): speed response, (**d**) Sectors in both strategies.

4. Conclusions

This paper provided an analytical investigation of the DTRFC algorithm over the entire speed range in terms of UnAs. The proposed scheme with (18) SSs is devised aimed to eliminate the UnAs of some VVs for medium and high speeds which yields a correct torque response. The transition speed value, at which the UnAs begin to appear, has been precisely analytically determined. Furthermore, the proposed method combined the advantages of conventional and improved strategies to work over a wide speed range. The simulation results validated the feasibility and effectiveness of the proposed scheme in IM drives over the wide speed range.

Artificial network techniques for the transition state between the two algorithms is the main goal for the future work.

Author Contributions: Conceptualization, M.M.A. and M.E.; methodology, M.M.A.; software, M.M.A.; validation, M.M.A., M.E. and F.A.; formal analysis, M.M.A.; investigation, M.M.A.; resources, M.E.; data curation, M.M.A., M.E. and F.A.; writing—original draft preparation, M.M.A.; writing—review and editing, M.M.A., M.E. and F.A.; visualization, M.M.A.; supervision, M.E. and F.A.; project administration, M.M.A.; funding acquisition, M.M.A. and M.E. All authors have read and agreed to the published version of the manuscript.

Funding: This research received no external funding.

Institutional Review Board Statement: Not applicable.

Informed Consent Statement: Not applicable.

Data Availability Statement: Not applicable.

Conflicts of Interest: The authors declare no conflict of interest.

Appendix A

Table A1. Parameters of three phase induction motor.

IM Parameters	Values
Nominal voltage	230/400[V]
Phase resistance stator	$R_s = 45.83[\Omega]$
Phase resistance rotor	$R_r = 31[\Omega]$
Phase inductance stator	$L_s = 1.24[H]$
Phase inductance rotor	$L_r = 1.11[H]$
Mutual inductance	$L_m = 1.05[H]$
Inertia	$J = 0.006[kg.m^2]$
Friction factor	f = 0.001[N.m.s/rad]
Number of poles pairs	p = 2
Nominal stator flux	$\Phi_s = 1.14[Wb]$
Nominal rotor flux	$\Phi_r = 0.945[Wb]$
Nominal power	$P_n = 0.25[kW]$
Nominal frequency	F = 50[Hz]
Nominal speed	$\omega_n = 282[rad/s]$
Nominal torque	$T_{em} = 1.76[N.m]$

References

1. Takahashi, I.; Noguchi, T. A New Quick-Response and High-Efficiency Control Strategy of an Induction Motor. *IEEE Trans. Ind. Appl.* **1986**, *IA-22*, 820–827. https://doi.org/10.1109/tia.1986.4504799.
2. Buja, G.; Kazmierkowski, M. Direct Torque Control of PWM Inverter-Fed AC Motors—A Survey. *IEEE Trans. Ind. Electron.* **2004**, *51*, 744–757. https://doi.org/10.1109/tie.2004.831717.
3. Idris, N.; Yatim, A. Direct Torque Control of Induction Machines With Constant Switching Frequency and Reduced Torque Ripple. *IEEE Trans. Ind. Electron.* **2004**, *51*, 758–767. https://doi.org/10.1109/tie.2004.831718.
4. Toh, C.; Idris, N.; Yatim, A. Constant and High Switching Frequency Torque Controller for DTC Drives. *IEEE Power Electron. Lett.* **2005**, *3*, 76–80. https://doi.org/10.1109/lpel.2005.851316.
5. Naassani, A.; Monmasson, E.; Louis, J.-P. Synthesis of Direct Torque and Rotor Flux Control Algorithms by Means of Sliding-Mode Theory. *IEEE Trans. Ind. Electron.* **2005**, *52*, 785–799. https://doi.org/10.1109/tie.2005.847581.

6. Nikzad, M.R.; Asaei, B.; Ahmadi, S.O. Discrete Duty-Cycle-Control Method for Direct Torque Control of Induction Motor Drives With Model Predictive Solution. *IEEE Trans. Power Electron.* **2017**, *33*, 2317–2329. https://doi.org/10.1109/tpel.2017.2690304.
7. Alsofyani, I.M.; Bak, Y.; Lee, K.-B. Fast Torque Control and Minimized Sector-Flux Droop for Constant Frequency Torque Controller Based DTC of Induction Machines. *IEEE Trans. Power Electron.* **2019**, *34*, 12141–12153. https://doi.org/10.1109/tpel.2019.2908631.
8. Meesala, R.E.K.; Thippiripati, V.K. An Improved Direct Torque Control of Three-Level Dual Inverter Fed Open-Ended Winding Induction Motor Drive Based on Modified Look-Up Table. *IEEE Trans. Power Electron.* **2019**, *35*, 3906–3917. https://doi.org/10.1109/tpel.2019.2937684.
9. Yang, G.; Yang, J.; Li, S.; Wang, Y.; Hussain, H.; Deng, R.; Yan, L. A Sequential Direct Torque Control Scheme for Seven-Phase Induction Machines Based on Virtual Voltage Vectors. *IEEE Trans. Ind. Appl.* **2021**, *57*, 3722–3734. https://doi.org/10.1109/tia.2021.3068932.
10. Wang, M.; Sun, D.; Ke, W.; Nian, H. A Universal Lookup Table-Based Direct Torque Control for OW-PMSM Drives. *IEEE Trans. Power Electron.* **2020**, *36*, 6188–6191. https://doi.org/10.1109/tpel.2020.3037202.
11. Wu, X.; Huang, W.; Lin, X.; Jiang, W.; Zhao, Y.; Zhu, S. Direct Torque Control for Induction Motors Based on Minimum Voltage Vector Error. *IEEE Trans. Ind. Electron.* **2020**, *68*, 3794–3804. https://doi.org/10.1109/tie.2020.2987283.
12. Nasr, A.; Gu, C.; Wang, X.; Buticchi, G.; Bozhko, S.; Gerada, C. Torque-Performance Improvement for Direct Torque-Controlled PMSM Drives Based on Duty-Ratio Regulation. *IEEE Trans. Power Electron.* **2021**, *37*, 749–760, https://doi.org/10.1109/tpel.2021.3093344.